AFRL-VA-WP-TP-2003-310

LONGITUDINAL CONTROL AND FOOTPRINT ANALYSIS FOR A REUSABLE MILITARY LAUNCH VEHICLE

Anhtuan D. Ngo and William B. Blake

APRIL 2003

AIR VEHICLES DIRECTORATE
AIR FORCE RESEARCH LABORATORY
AIR FORCE MATERIEL COMMAND
WRIGHT-PATTERSON AIR FORCE BASE, OH 45433-7542

20030516 050

REPORT DOCUMENTATION PAGE

Form Approved
OMB No. 0704-0188

1. REPORT DATE (DD-MM-YY)	2. REPORT TYPE	3. DATES COVERED (From - To)
April 2003	Conference Paper Preprint	

4. TITLE AND SUBTITLE	5a. CONTRACT NUMBER
LONGITUDINAL CONTROL AND FOOTPRINT ANALYSIS FOR A REUSABLE MILITARY LAUNCH VEHICLE	In-house
	5b. GRANT NUMBER
	5c. PROGRAM ELEMENT NUMBER N/A

6. AUTHOR(S)	5d. PROJECT NUMBER N/A
Anhtuan D. Ngo and William B. Blake	5e. TASK NUMBER N/A
	5f. WORK UNIT NUMBER N/A

7. PERFORMING ORGANIZATION NAME(S) AND ADDRESS(ES)	8. PERFORMING ORGANIZATION REPORT NUMBER
Control Theory Optimization Branch (AFRL/VACA) Control Sciences Division Air Vehicles Directorate Air Force Research Laboratory, Air Force Materiel Command Wright-Patterson Air Force Base, OH 45433-7542	AFRL-VA-WP-TP-2003-310

9. SPONSORING/MONITORING AGENCY NAME(S) AND ADDRESS(ES)	10. SPONSORING/MONITORING AGENCY ACRONYM(S)
Air Vehicles Directorate Air Force Research Laboratory Air Force Materiel Command Wright-Patterson Air Force Base, OH 45433-7542	AFRL/VACA
	11. SPONSORING/MONITORING AGENCY REPORT NUMBER(S) AFRL-VA-WP-TP-2003-310

12. DISTRIBUTION/AVAILABILITY STATEMENT
Approved for public release; distribution is unlimited.

13. SUPPLEMENTARY NOTES
To be presented at the American Institute of Aeronautics & Astronautics - GNC, Austin, TX, August 9-15, 2003.
This material is declared a work of the U.S. Government and is not subject to copyright protection in the United States.

14. ABSTRACT

In this paper, we will examine a configuration for a reusable military launch vehicle (RMLS) concept. This configuration allows for the vehicle to land in an inverted attitude. Such inverted landing improves the turnaround time of the vehicle by reducing the maintenance requirements of the vehicle's thermal protection system. An analysis is performed to examine the impacts by the configuration on stability, control, and footprint for an RMLS configuration.

15. SUBJECT TERMS
downrange, crossrange, footprint Euler-Lagrange Method, maximum attainable moments

16. SECURITY CLASSIFICATION OF:			17. LIMITATION OF ABSTRACT:	18. NUMBER OF PAGES	19a. NAME OF RESPONSIBLE PERSON (Monitor)
a. REPORT	b. ABSTRACT	c. THIS PAGE	SAR	14	Anhtuan D. Ngo
Unclassified	Unclassified	Unclassified			19b. TELEPHONE NUMBER (Include Area Code) (937) 255-8494

Standard Form 298 (Rev. 8-98)
Prescribed by ANSI Std. Z39-18

i

Longitudinal Control and Footprint Analysis for a Reusable Military Launch Vehicle

Anhtuan D. Ngo and William B. Blake

Air Force Research Laboratory/VACA

2210 Eighth Street, Bldg 146

Wright-Patterson AFB, OH. 45433-7531

Email: anhtuan.ngo@va.afrl.af.mil/william.blake@va.afrl.af.mil

Abstract

In this paper, we will examine a configuration for reusable military launch vehicle (RMLS) concept. This configuration allows for the vehicle to land in an inverted attitude. Such inverted landing improves the turn-around time of the vehicle by reducing the maintenance requirements of the vehicle's thermal protection system. An analysis is performed to examine the impacts by the configuration on stability, control and footprint for an RMLS configuration.

1 Introduction

In recent years, the increasing potential of space in military and commercial applications has attracted interest in space operation vehicles by governments and industries. The renewed interest has resulted in various design studies and engineering development programs such as NASA's X-34 hypersonic rocket powered test vehicle, and X-37 reusable upper stage and satellite bus, X-33 program for demonstrating single-stage to orbit, the Ballistic Missile Defense Organization's Single-Stage Rocket Technology program that built the Delta Clipper-Experimental (DC-X) experimental reusable spaceplane. The objectives of these design studies and engineering programs are to advance the technologies required for affordable and reliable space flights such as composite propellant tanks, lightweight robust airframe, long life-time thermal protection system. Furthermore, to make space access more routine, NASA's Space Launch Initiative (SLI) aims to develop a second generation reusable launch vehicle that reduces cost while improving safety and reliability. Parallel to NASA's effort in meeting requirements of reusable launch vehicles for civilian applications is the Department of Defense's National Aerospace Initiative (NAI) which seeks to meet the unique requirements of military space operation vehicles such as launch-on-demand along with affordability, safety, and reliability. As a result, increasing focus is placed on technolo-

gies that enable the space vehicles to have aircraft-like characteristics such as safety, operability, supportability, turn-around-time, and affordability. Supporting this space effort to meet the goals of future military space operation vehicles, a design study for a reusable military launch vehicle is performed at the Air Force Research Laboratory to examine the operations, capabilities, trajectories, stability and control of a military reusable launch vehicle. In this paper, we will examine an innovative vehicle concept that eliminates several of the factors that currently contribute to high turnaround times and its impacts on stability, control and footprint for an RMLS configuration.

2 Longitudinal Stability Prediction

Missile Datcom (Ref. [1]) was used to calculate the longitudinal aerodynamic characteristics of the vehicle. Missile Datcom is a widely used engineering-level code that uses the component buildup technique to predict vehicle aerodynamics. Code input consists of body, wing and tail geometry, Mach number, altitude, angle of attack and control deflections. Control devices are limited to either all moving controls or plain trailing edge flaps. At each flight condition the six-body axis force and moment coefficients are provided. Both theoretical and empirical methods are included that encompass the entire speed regime from subsonic to hypersonic. An improved method for calculating the center of pressure of a wing with a large strake (typical of many re-entry vehicles) was recently incorporated (Ref [2]). Missile Datcom has been shown to provide very good agreement with experimental data for a variety of missile configurations (Ref. [3]). To validate the code for RLV type configurations, extensive comparisons have been made with wind tunnel data for the X-34 and X-40 configurations. Sample results for the X-34 shown in Fig 1 (Ref. [4]) will be given here. Lift coefficient is predicted very well at both transonic and hypersonic speeds, as indicated in Figure 2. The large reduction in lift curve slope at hypersonic speeds

is evident. Pitching moment comparisons are shown in Figure 3. At hypersonic speeds, both the prediction and data show that the configuration is unstable at low angles of attack and becomes stable at the high angles of attack attained during re-entry. At transonic speeds, the configuration is very stable with an unstable break between 10 and 20 degrees. Although Missile Datcom correctly predicts the slope and the break, the zero angle of attack value is underpredicted. This is probably because the code ignores the effect of forebody camber. The overall shift in static stability represents a center of pressure travel of about 6 percent of the body length.
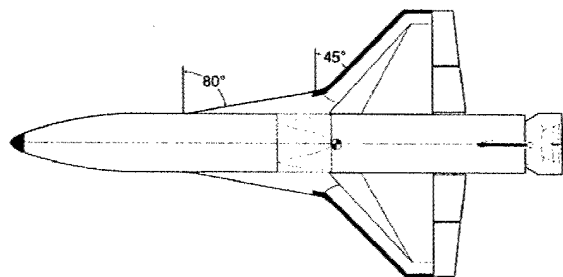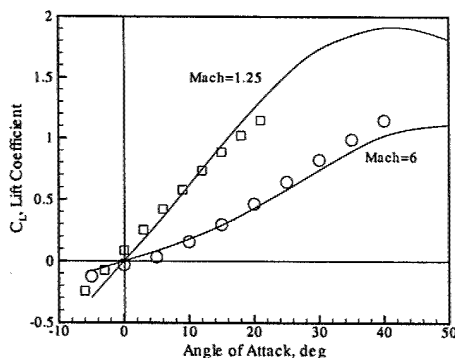

Figure 1: X-34 Reusable Launch Vehicle

Figure 2: X-34 Lift Coefficient Comparison

3 Reusable Military Launch Vehicle

A USAF X-42 design is the study vehicle for the present paper (Figures 4-6). The X-42 is a proposed Air Force Research Laboratory Technology Demonstrator currently under study. It is a scaled version of a reusable military launch system and is intended to demonstrate technologies for rapid turnaround launch concepts. The basic requirement for the X-42 is to place a 1000 lb payload into low earth orbit. The baseline design is a single stage, vertical takeoff horizontal
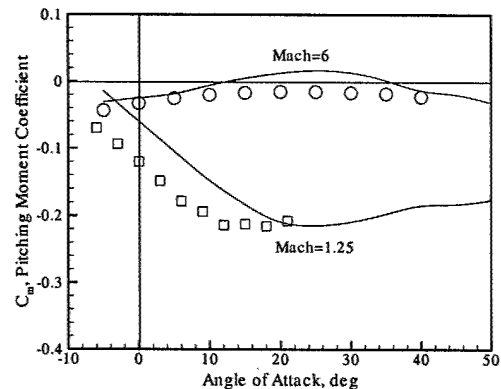

Figure 3: X-34 Pitching Moment Coefficient Comparison

landing vehicle powered by 4 NK-39 rocket engines. It has a gross weight of 168,000 lb, and empty weight of 28,000 lb, is 53 ft long, 10 ft in diameter, and has a 39 ft wing span. The relatively low fineness ratio enhances accessibility and operability features. The vehicle has five control effectors, an elevon on each wing, a body flap below the rocket nozzles, and rudders on the wing tip mounted vertical tails. The tip mounted tails endplate the wing at subsonic speeds, increasing lift and decreasing landing speed.

Predicted lift (L), drag (D) and L/D characteristics of the vehicle at subsonic, transonic and hypersonic speeds are shown in Figures 7-10. The lift and drag characteristics are similar to both the Space Shuttle and X-34, with a lift curve slope of about 4/radian at low speeds which decreases significantly at hypersonic speeds. The angle of attack for maximum lift increases with increasing Mach number, from 30 degrees at Mach 0.3 to 50 degrees at Mach 20. The maximum lift to drag ratio (Figure 10) decreases from about 4.5 at subsonic speeds to just over 1 at hypersonic speeds. At hypersonic speeds, the typical flight angle of attack ($\sim$ 35 deg) is much higher than the predicted angle of attack for maximum L/D.
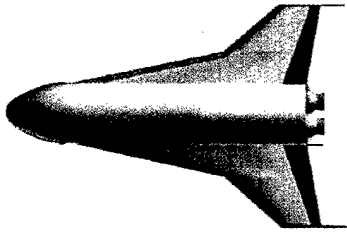

Figure 4: X-42-A Side View

Figure 5: X-42-A Top View

Figure 6: X-42-A With a Payload

Figure 7: X-42 Lift and Drag Coefficients at Mach 0.3
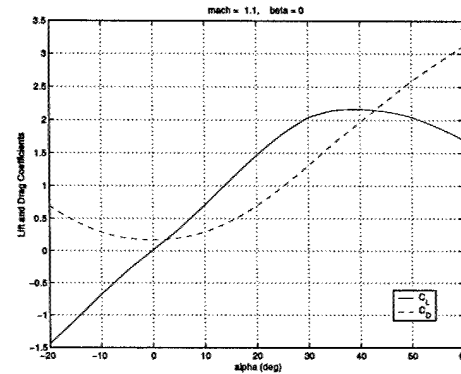
Figure 8: X-42 Lift and Drag Coefficients at Mach 1.1

3.1 Inverted Landing

One of the primary goals of the RMLS study is to attain a high launch rate, which can be measured by time between launches of a given vehicle. The current goal is 12 hours between launches, which is far less than the 3 month turnaround time for the Space Shuttle. One idea that addresses two of the problems that contribute to the Space Shuttle's long turn time is to land the aircraft in an inverted attitude. The idea of an inverted landing is not new, inverted landers were studied during the NASP era to address inlet integration problems.

One of the major maintenance items on the Space Shuttle is the thermal protection system (TPS) on the bottom of the vehicle. The tiles and seals that compose the TPS must be laboriously inspected and replaced in many cases after each mission. One major problem area is the seals around the landing gear doors. Placing the landing on the top of the vehicle would remove the need for these seals, reducing TPS maintenance requirements.

The tires and brakes on the Space Shuttle must be replaced after every flight due to excessive wear from high speed landings. An inverted landing would change the body camber from nose down to nose up. The control deflection required to trim this camber change increases lift, which decreases landing speed. Trimmed lift as a function of angle of attack can be written as:

$$C_L = C_{L_o} + C_{L_\alpha}\alpha + C_{L_\delta}\delta - \frac{C_{L_\delta}}{C_{m_\delta}}(C_{m_o} + C_{m_\alpha}\alpha)$$

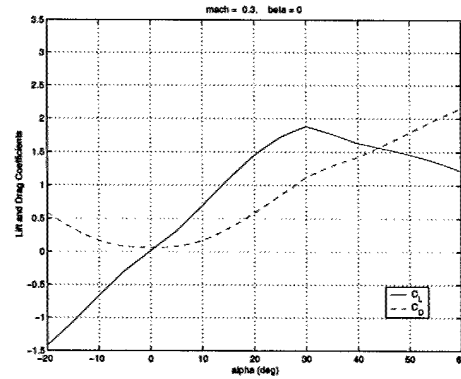Inverting the vehicle simply changes the sign of the Clo and Cmo terms, so the incremental lift can be written

as:

$$\Delta C_L = 2[C_{m_o}\frac{C_{m_\delta}}{C_{m_\delta}} - C_{L_o}]$$

This increment will be reduced by ground effects, since inverting the vehicle moves the wing away from the ground.

$$
\begin{aligned}
C_L &= C_{L_o} + C_{L_\alpha}\alpha + C_{L_\delta}\delta \\
C_m &= C_{m_o} + C_{m_\alpha}\alpha + C_{m_\delta}\delta \\
C_L &= C_{L_o} + C_{L_\alpha}\alpha - \frac{C_{L_\delta}}{C_{m_\delta}}(C_{m_o} + C_{m_\alpha}\alpha) \\
\Delta C_L &= 2[C_{m_o}\frac{C_{m_\delta}}{C_{m_\delta}} - C_{L_o}]
\end{aligned}
$$

3.2 Longitudinal Stability and Control Effectiveness Comparison

The ability of the vehicle to maintain its longitudinal equilibrium is required before any maneuver is performed by the vehicle. It is therefore of interest to examine the ability of the control surfaces of the vehicle to zero out the wing-body pitching moment so that the equilibrium equations is satisfied:

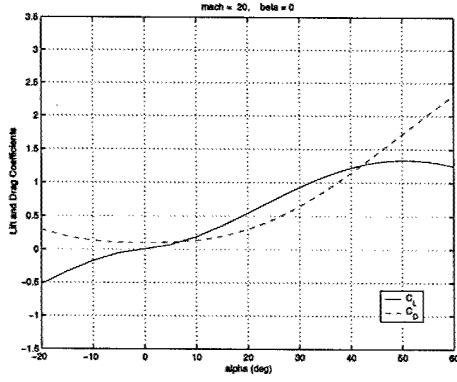$$M_o(\alpha, \beta, \mathrm{M}) + M_\delta(\alpha, \beta, \mathrm{M}) = 0 \qquad (1)$$

Figure 9: X-42 Lift and Drag Coefficients at Mach 20
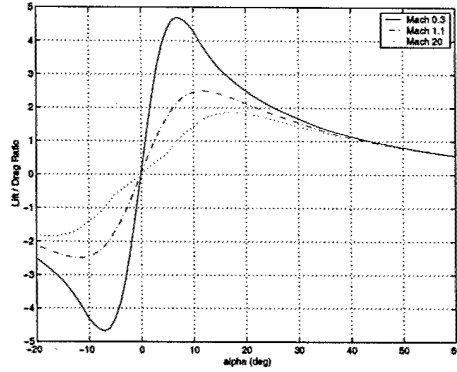
Figure 10: X-42 $\frac{L}{D}$ at Mach 0.3,1.1, 20

Figure 11: X-42 Pitching Moment Coefficients at Mach 0.3
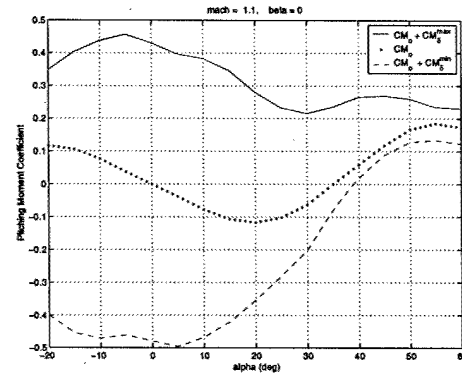
Figure 12: X-42 Pitching Moment Coefficients at Mach 1.1

We note that in Equation 1, the wing-body pitching moment M_o and total control effector pitching moment M_δ can be written as

$$M_0 = \frac{1}{2}\rho v^2 \bar{c} S C_{M_0}$$

$$M_\delta = \frac{1}{2}\rho v^2 \bar{c} S C_{M_\delta}$$

where ρ is the air density, v is the velocity, S is the plane form area, $\bar{c}$ is the mean aerodynamic chord, C_{M_o} is the wing-body pitching coefficient, C_{M_δ} is the total control pitching coefficient. The control pitching coefficient can be further expressed as

$$C_{M_\delta} = C_{M_{\delta_1}} + \cdots + C_{M_{\delta_m}}$$

The upper bound $\overline{C}_{M_\delta}$ and lower bound $\underline{C}_{M_\delta}$ of C_{M_δ} can be expressed as

$$\overline{C}_{M_\delta} = \overline{C}_{M_{\delta_1}} + \cdots + \overline{C}_{M_{\delta_m}}$$
$$\underline{C}_{M_\delta} = \underline{C}_{M_{\delta_1}} + \cdots + \underline{C}_{M_{\delta_m}}$$

where over the range of each control effector δ_i, e.i. $\underline{\delta}_i \leq \delta_i \leq \overline{\delta}_i$, we have

$$\overline{C}_{M_{\delta_i}} = \max_{\delta_i} C_m(\delta_i)$$

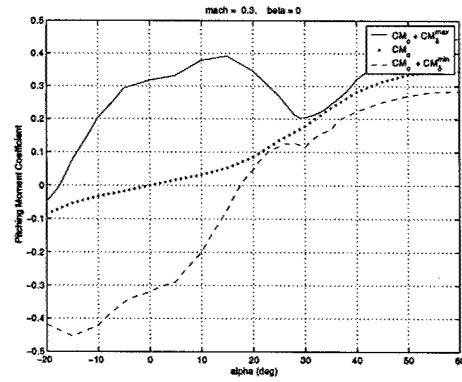$$\underline{C}_{M_{\delta_i}} = \min_{\delta_i} C_m(\delta_i)$$

Thus at a given sideslip angle β, and Mach number M, and an angle of attack α, the flight condition is trimmable if

$$C_{M_o}(\alpha,\beta,\text{M}) + \overline{C}_{M_\delta}(\alpha,\beta,\text{M}) \geq 0$$
$$\text{and} \qquad (2)$$
$$C_{M_o}(\alpha,\beta,\text{M}) + \underline{C}_{M_\delta}(\alpha,\beta,\text{M}) \leq 0$$

Figures 11, 12, and 13 show the pitching moment coefficient C_{M_o} along with residual pitching moment's upper bound $(C_{M_o} + \overline{C}_{M_\delta})$ and lower bound $(C_{M_o} + \underline{C}_{M_\delta})$ at zero sideslip, i.e. $\beta = 0$, over a range of angles of attach α for different Mach numbers. These figures show that the vehicle is statically unstable at low angles of attack at both subsonic and hypersonic speeds, and stable at transonic speeds. At Mach = 0.3, the amount of instability at low speeds is low and should be easily accommodated by a flight control system. For a dynamic pressure of 300 psf, unlikely to be exceeded during approach, the time to double amplitude of the pitch instability is about 0.9 sec. At Mach = 20, there is a stable break in the pitching moment curve at about
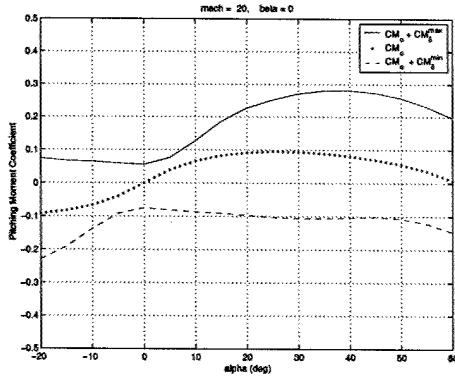
Figure 13: X-42 Pitching Moment Coefficients at Mach 20

25 degrees angle of attack. This shows that the vehicle would be stable for a typical re-entry (AOA $\sim$ 35 deg). Both the X-34 (Ref. [4]) and Space Shuttle (Ref. [5]) have a similar characteristic.

Using the equilibrium requirements in (2), the trimmable angles of attack can be found from these figures. Table 1 summarizes the range of trimmable angles of attack. Using this range of trimmable angles of

Table 1: Range of Trimmable Angles of Attack

Mach Number	α_{trim} (X-42)
0.3	$-17°$ to $18°$
0.9	$-20°$ to $26°$
1.1	$-20°$ to $39°$
20	$-20°$ to $60°$

attack, we can then find the condition in which the vehicle is trimmed in its angular attitude, balanced with lift being equal to its weight, and encounters the least drag. In the next section, we will see how these factors affect the vehicle reachable region under no power.

3.3 Footprint Calculation

The vehicle is assumed to be stabilized with an inner loop attitude controller, the dynamic equations for the un-powered vehicle over a non-rotating earth can be written as:

$$\dot{h} = v\sin(\gamma) \tag{3}$$

$$\dot{\theta} = \frac{v\cos(\gamma)\cos(\psi)}{(R_o + h)} \tag{4}$$

$$\dot{\phi} = \frac{v\cos(\gamma)\sin(\psi)}{(R_o + h)} \tag{5}$$

$$\dot{v} = \frac{-D}{m} - \frac{\mu\sin(\gamma)}{(R_o + h)^2} \tag{6}$$

$$\dot{\gamma} = \frac{L\cos(\sigma)}{mv} - \frac{\mu\cos(\gamma)}{v(R_o + h)^2} + \frac{v\cos(\gamma)}{(R_o + h)} \tag{7}$$

$$\dot{\psi} = \frac{L\sin(\sigma)}{mv\cos(\gamma)} - \frac{v\cos(\gamma)\cos(\psi)\tan(\phi)}{(R_o + h)} \tag{8}$$

Where

h	:	Altitude
θ	:	Longitude
ϕ	:	Latitude
v	:	Velocity
γ	:	Flight path angle
ψ	:	Heading angle
m	:	Mass of the vehicle
R_o	:	Earth's Radius
μ	:	Gravitational Parameter

Figure 14 illustrates the coordinate system used to model the vehicle.
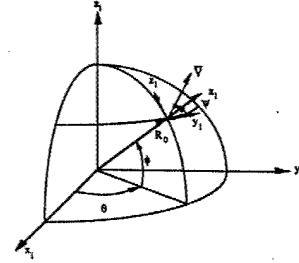

Figure 14: Coordinates System

Induced aerodynamic drag and friction acting on the vehicle, cause the total energy of the un-powered vehicle to be monotonically decreasing. The vehicle footprint then consists of points on the earth's surface at which the total energy decreases to a set value. When its energy reaches this value, the vehicle then enters the final part of its trajectory called terminal area energy management phase. Combining its velocity v and altitude h in an energy-state approximation [6], a reduced order model can be obtained to simplify the vehicle description. The specific energy of the vehicle can be expressed as

$$E = \frac{1}{2}v^2 + \frac{\mu}{(R_o + h)^2}h \tag{9}$$

From equations 3, 6, and 9, the rate of decrease in the vehicle's energy is

$$\frac{dE}{dt} = -\frac{vD}{m} - \frac{2\mu hv\sin(\gamma)}{(R_o + h)^3} < 0 \tag{10}$$

Assuming that the vertical forces acting on the vehicles are in equilibrium and its vertical motion frequency dynamics are much faster its horizontal motion dynamics, the flight path angle can be taken to be near zero, i.e., $\gamma \approx 0$. Moreover, since the acceleration normal to the velocity vector is small, i.e., $(v\dot{\gamma} \approx 0)$ and $v \neq 0$, the time-rate of change of the flight path angle can then be taken to be essentially zero, i.e., $\dot{\gamma} \approx 0$. From equation 7, we have

$$L = \frac{m}{cos(\sigma)} \left(\frac{\mu}{(R_o + h)^2} - \frac{v^2}{(R_o + h)} \right) \qquad (11)$$

With

$$L = \frac{1}{2}\rho v^2 S_a C_L \qquad (12)$$

$$D = \frac{1}{2}\rho v^2 S_a C_D, \text{ and } C_D = C_{D_o} + kC_L^2 \qquad (13)$$

we can combine equations 11 and 12 into equation 13 to get

$$D = \frac{1}{2}\rho v^2 S_a C_{D_o} + \frac{2m^2 k\tilde{g}^2}{\rho v^2 S_a \cos^2 \sigma} \qquad (14)$$

where $\tilde{g}$ is the effective gravity constant:

$$\tilde{g} = \frac{\mu}{R_o + h} - \frac{v^2}{R_o + h}$$

Given the initial velocity $v(t_o) = v_o$, and initial altitude $h(t_o) = h_o$, the vehicle specific energy $E(t)$ can be calculated according equation 10:

$$E(t) = E_o + dE = \frac{1}{2}v_o^2 + \frac{\mu h_o}{(R_o + h)^2} + dE \qquad (15)$$

The vehicle's velocity $v(t)$ can be derived from the current specific energy $E(t)$:

$$v(t) = \sqrt{2E(t) - \frac{\mu h}{(R_o + h)^2}} \approx \sqrt{2E(t)} \qquad (16)$$

since the vehicle flight altitude h is small when compared to the earth's radius R_o. From the above discussion, the unpowered vehicle under energy-state approximations has the reduced-order model $\dot{x} = f(x, u, t)$ of the form:

$$\dot{\theta} = \frac{v\cos(\psi)}{(R_o + h)\cos(\phi)} \qquad (17)$$

$$\dot{\phi} = \frac{v\sin(\psi)}{R_o + h} \qquad (18)$$

$$\dot{\psi} = \frac{z\tilde{g}}{v} - \frac{v\cos(\psi)\tan(\phi)}{R_o + h} \qquad (19)$$

$$\dot{E} = \frac{-Dv}{m} \qquad (20)$$

where $x = [\theta, \phi, \psi, E]^T$ is the vehicle state vector. The control inputs $u = [\rho \quad z]^T$ are the air density, $\rho = \rho(h)$, and the tangent of the bank angle,

$z = \tan(\sigma)$. The optimization objective is to find the control vector $u = [\rho \quad z]$ such that, at time $t = t_f$, the crossrange position specified by the vehicle latitude $\phi(t_f)$ is maximized for a given downrange value $\theta_f = \theta(t_f)$:

$$\max_{\rho, z} J = \int_{t_o}^{t_f} G \, dt = \int_{t_o}^{t_f} -\dot{\phi} \, dt \qquad (21)$$

The initial values of the vehicle states are taken to be $\theta(t_o) = 0$, $\phi(t_o) = 0$, $\psi(t_o) = 0$ and $E(t_o) = E_o$. Following a similar derivation for the optimal control vector z as shown in [7], we have

$$\rho_{opt} = \sqrt{\frac{4m^2 k\tilde{g}^2 (1 + z^2)}{v^2 S_a C_{do}}} \qquad (22)$$

The optimum bank angle σ associated with $z = \tan(\sigma)$ is

$$z_{opt} = \frac{\cos(\phi)\sin(\tilde{\theta})(\frac{\mu}{R^2} - \frac{v^2}{R})\frac{R}{v^2}}{\cos(\tilde{\theta})\sin(\psi) - \sin(\phi)\sin(\tilde{\theta})\cos(\psi)} \qquad (23)$$

$$\tan(\theta_f) = \tan(\theta'_f)\cos(\psi'_o) + \frac{\tan(\phi'_f)\sin(\psi'_f)}{\cos(\theta'_f)}$$

$$\sin(\phi_f) = \sin(\phi'_f)\cos(\psi'_o) - \sin(\theta'_f)\cos(\phi'_f)\sin(\psi'_f)$$

Equations 22 and 23 give the optimal cross-range $\phi(t_f)$ for a given downrange θ_f. Iterations on the initial values of θ_f may be necessary so that the initial guess matches the final value $\theta(t_f)$ resulted from the equations 20.

4 Application to a Reusable Launch Vehicle

In this section, we apply the method for the footprint calculation to the X-42 reusable launch vehicle. At the beginning of the reentry phase, the 870-slug vehicle attains the velocity of $12,500$ feet/second at an altitude of $210,000$ feet. With this initial energy, the unpowered vehicle's crossrange is calculated until its final energy is equivalent to the energy at the final speed of 1500 feet/second and $60,000$ feet of altitude. The air density constraint which is related to thermal constraint on the vehicle is $\rho < 7.397 \times 10^{-5}$slugs/ft^3. Similarly, structure-related air density constraint has an upper limit of 3.981×10^{-5}slugs/ft^3.

An important requirement that must be satisfied in calculating the vehicle footprint is the maintenance of lift to effective-weight equilibrium (L=W) while banking the vehicle:

$$L = \frac{1}{2}\rho^2 S_a C_L = W = \frac{m\tilde{g}}{\cos(\sigma)}$$

where S_a is vehicle planform area and ρ is the air density. The respective normal and axial force coefficients C_N and C_A obtained from the vehicle's aerodynamic table are transformed into the corresponding lift and drag coefficients C_L and C_D:

$$C_L = \cos(\alpha)C_N - \sin(\alpha)C_A$$
$$C_D = \sin(\alpha)C_N + \cos(\alpha)C_A$$

A root solver based on the Secant method is then used to minimize the residual of $L - W$. Scanning the altitude that is $20,000$ feet above and below the vehicle's current altitude, we look for the next optimal altitude command that minimizes the vehicle's drag subject to the constraint $L = W$. In addition to.ensuring that the lift on the vehicle equals its weight, rotational equilibrium must also be enforced to maintain the vehicle's attitude. A trim routine is used to find the aero-control positions that are necessary to balance the base pitching moment produced by the wing-body portion of the vehicle. The lateral directional moments resulting from the wing-body portion of the vehicle are assumed to be zero (i.e. an assumption of zero steady-state sideslip and wing-body symmetry). In the trim routine, the roll, pitch and yaw control effectiveness of each aero-control surface at a fixed Mach number and angle of attack is found from the aerodynamic table using small perturbations. With B being the pitch control effectiveness matrix, δ the aero-control deflections and M_o the base pitching moment, a linear programming formulation [8] is used to find δ such that:

$$\min_{\delta} J = \|B\delta - M_o\|_1 \qquad (24)$$
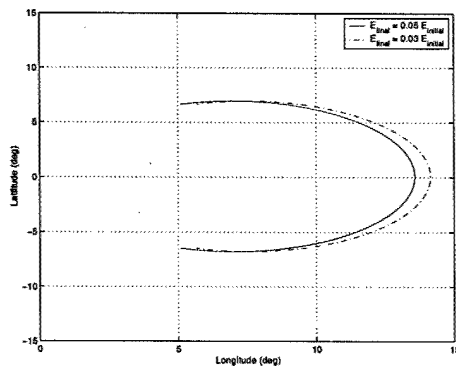$$\text{subject to} \quad \underline{\delta} \leq \delta \leq \overline{\delta}$$

Figure 15: X-42-B Side View

5 Conclusion

In this paper, we have examine the stability and control effectiveness of a configuration for a reusable military launch vehicle. The novel configuration enables the vehicle to land in inverted attitude which has a potential to reduce maintenance requirements of the thermal protection system. The vehicle is found to have a large range of trimmable angle of attack at different Mach numbers. Also, the footprint of the vehicle is also examined so that in the event of an emergency a landing site can be chosen according to its current velocity and altitude.

6 Acknowledgement

References

[1] Blake, W.B., "Missile Datcom User's Manual - 1997 Fortran 90 Revision," *AFRL-VA-WP-TR-1998-3007*, March 1998.

[2] Blackmar, S., Miller, M., and Blake, W., "Approximate Methods for Center of Pressure Prediction of Multi-Segment Wings" *Proceedings of the 2003 Applied Aerodynamics Conference*, AIAA 2003-xxxx, June 2003 (to be presented).

[3] Packard, J, and Miller, M.,"Assessment of Engineering Level Codes for Missile Aerodynamic Design and Analysis" *Proceedings of the 2000 Atmospheric Flight Mechanics Conference*, AIAA 2000-4590, Aug. 2000.

[4] Brauckmann, G.J.,"X-34 Vehicle Aerodynamic Characteristics" *Journal of Spacecraft and Rockets*, Vol. 36, No. 2., 1999, pp. 229-239.

[5] Young, J.C., et al, "The Aerodynamic Challenges of the Design and Development of the Space Shuttle Orbiter" NASA CP 2342 (Part 1), pp. 209-263, January 1985.

[6] E. S. Rutowski, "Energy Approach to the General Aircraft Performance Problem," *Journal of Aeronautical Sciences* Vol. 21, 1954, pp. 187-195.

[7] Ngo, A. D., Doman D.B, "Footprint Calculation Methods for a Reusable Launch Vehicle," ACC02-AIAA1032, American Control Conference (ACC-2002), Anchorage, Alaska, May 2002

[8] D. B. Doman, A. D. Ngo, D. B. Leggett, M. A. Saliers, "Development of A Hybrid Direct-Indirect Adaptive Control System for the X-33," in *Proceedings of the 2001 Guidance, Navigation and Control Conference*, AIAA 2001-4156, Aug. 2001.